Heliyon 10 (2024) e24762

Contents lists available at ScienceDirect

Heliyon

journal homepage: www.cell.com/heliyon

Research article

Constrained numerical deconvolution using orthogonal polynomials

J.M. Maestre [a,b,*], P. Chanfreut [c], L. Aarons [d]

[a] Department of Systems and Automation Engineering, University of Seville, Spain
[b] Health and Pharmacy PhD program at University of Salamanca, Spain
[c] Department of Mechanical Engineering, Eindhoven University of Technology, the Netherlands
[d] Division of Pharmacy and Optometry, The University of Manchester, Manchester, UK

A B S T R A C T

In this article, we present an enhanced version of Cutler's deconvolution method to address the limitations of the original algorithm in estimating realistic input and output parameters. Cutler's method, based on orthogonal polynomials, suffers from unconstrained solutions, leading to the lack of realism in the deconvolved signals in some applications. Our proposed approach incorporates constraints using a ridge factor and Lagrangian multipliers in an iterative fashion, maintaining Cutler's iterative projection-based nature. This extension avoids the need for external optimization solvers, making it particularly suitable for applications requiring constraints on inputs and outputs. We demonstrate the effectiveness of the proposed method through two practical applications: the estimation of COVID-19 curves and the study of mavoglurant, an experimental drug. Our results show that the extended method presents a sum of squared residuals in the same order of magnitude of that of the original Cutler's method and other widely known unconstrained deconvolution techniques, but obtains instead physically plausible solutions, correcting the errors introduced by the alternative methods considered, as illustrated in our case studies.

1. Introduction

Deconvolution plays a crucial role in various scientific disciplines [7,17]. Its primary goal is to recover an *original* signal from an *observed* signal convoluted with a known system response or filter function [34]. Therefore, deconvolution can be thought of as inverting the system response on the observed signal so as to accurately recreate the original one. Recovering this information can provide a deeper understanding of the process under consideration and enhance decision-making in diverse applications. For instance, in geophysics, deconvolution is used to estimate information about the Earth's subsurface from measured seismic signals [39,35]; in astronomy, it is used to remove atmospheric seeing degradation to obtain clearer images [38]; and in biomedical engineering one can find multiple applications, e.g., identifying types of cells [31,25,20] and In Vitro–In Vivo Correlations (IVIVC) [21], and finding the time profile in which insulin enters the blood after subcutaneous injections [36,9].

Numerous techniques have been proposed to tackle the deconvolution problem, ranging from numerical methods to optimization-based approaches [38]. In addition, according to the way the input signal is deconvolved, it is possible to classify the methods that appear in the literature in three different categories: parametric approaches, i.e., methods assuming a functional form of the input whose parameters are unknown [12,42,23]; nonparametric approaches, i.e., methods that estimate the input signal without any prior assumption on its shape or time evolution [33,14,37]; and semiparametric approaches, i.e., methods that combine features of the two categories presented above [43,11]. However, many decovolution methods suffer from issues such as computational complexity,

* Corresponding author.
E-mail addresses: pepemaestre@us.es (J.M. Maestre), p.chanfreut.palacio@tue.nl (P. Chanfreut), leon.aarons@manchester.ac.uk (L. Aarons).

https://doi.org/10.1016/j.heliyon.2024.e24762
Received 18 July 2023; Received in revised form 28 December 2023; Accepted 14 January 2024

Available online 18 January 2024

parameter tuning, and ill-conditioning [40,39,31], mainly when they rely on the inversion of the convolution matrix, which can be ill-conditioned or even singular.

In this article, our primary objective is not simply to find an estimation of the input vector, but rather to extend and improve upon a parametric deconvolution method in a least-square sense for linear systems introduced by Cutler in 1978 [11]. This method is based on the use of orthogonal polynomials to project the observed signal onto the span of a set of basis vectors. By leveraging orthogonal polynomials, this method offers: i) improved numerical stability in calculations, minimizing the impact of small errors in the deconvolved signal; ii) improved noise resistance, leading to cleaner estimates of the underlying functions; iii) better handling of complex patterns, ensuring more accurate reconstructions than other methods; and iv) additional flexibility in the deconvolution process through the choice of specific orthogonal polynomials (e.g., Legendre [46], Racah [26], Hermite, Chebyshev, etc.) [32,2,15].

Indeed, the use of orthogonal polynomials simplifies the computation of input coefficients and helps avoid numerical issues that can plague other methods. Nevertheless, the original Cutler method remains unconstrained, which can lead to unrealistic parameter estimates, such as physiological signals that should be positive becoming negative at specific time points. To bridge this gap, our primary contribution is introducing constraints to improve upon Cutler's original approach. Specifically, we focus on enhancing its applicability by ensuring the derived deconvolution results are more physically realistic. To this end, we propose two principal extensions to the Cutler method:

1. Incorporating a ridge factor to regularize the solution: This is a standard approach that introduces a tuning parameter to control the smoothness of the deconvolved signal, providing a way to minimize the impact of noise or other irregularities in the signal in order to obtain a more realistic and stable output.
2. Using Lagrange multipliers in an iterative fashion to deal with the constraints: Lagrangian multipliers allow us to address constraint violations explicitly through a cost function, providing a mechanism that ensures that deconvolved signals adhere to predefined conditions so that they are physically plausible.

While other alternatives might be possible, e.g., using the gradient projection method [10,13], we believe that the proposed approach is more natural as it maintains the simplicity and iterative nature of the original Cutler's approach. As will be seen, the proposed method does not rely on complex computations, but on straightforward loops and scalar products. At this point, it is necessary to remark that we do not aim to establish the superiority of our method over others, but rather to present a valid alternative that is simple to understand, implement, and well-suited to applications where constraints are required. That is, while there may be existing methods that could potentially serve this purpose, by extending Cutler's algorithm we contribute to the toolbox of techniques available to the broader scientific community.

To demonstrate the practical relevance and applicability of our approach, the extended Cutler method is applied to two real-world examples. In the first example, we apply the method to COVID-19 curves, reconstructing the underlying dynamics of the pandemic and providing valuable insights into the evolution of the virus. This application is particularly relevant in the context of recent studies that have used deconvolution techniques to analyze the spread of infectious diseases [28,30]. In the second example, we apply our method to the study of mavoglurant, a drug used to treat neurological disorders. Here, the extended Cutler method is used to estimate the pharmacokinetic profile of the drug, helping researchers to better understand its absorption process. In this context, we also provide comparisons with other existing deconvolution techniques to illustrate the performance of our proposed method in the presence of noise, ill-conditioning, and other challenges.

The structure of this article is as follows. In Section 2, we introduce the mathematical framework and notation for the deconvolution problem, followed by a detailed explanation of the original Cutler's method. In Section 3, the proposed extensions to the Cutler method are presented. In Section 4, we present numerical simulations, and Section 5 provides concluding remarks and discusses future research directions.

2. Problem setting and some classical methods for numerical deconvolution

Consider a discrete-time single-input single-output system with linear and time-invariant dynamics. For this class of systems, the dynamics can be modeled using its impulse response $g = [g_0, g_1, \dots]^\top$, which here is assumed to be finite. Here, g_k denotes the value of the signal at time instant k. Note that with a certain abuse of notation we have written the discrete-time signal g as a vector. The reason to do that will become clearer later.

In general, given an input u and the impulse response g, the output of the system, say y, can be written as

$$\begin{aligned} y_k = (g * u)[k] &= \sum_{t=-\infty}^{k} u_{k-t} g_t \\ &= \sum_{t=-\infty}^{k} g_{k-t} u_t, \end{aligned} \tag{1}$$

where k is the discrete-time index and the operator $*$ stands for convolution. An intuitive way to understand what convolution means is to think of the input u as a sum of scaled impulse functions. Since the system is linear and time-invariant, the superposition principle allows us to express the output y as the sum of the corresponding scaled impulse responses of the system.

Considering that both u_k and g_k are zero for $k < 0$ and that all these signals can be observed until time instant $k = S$,[1] it is possible to rewrite Eq. (1) in an algebraic manner as

$$\mathbf{y} = G\mathbf{u}, \tag{2}$$

where

$$\mathbf{y} = \begin{bmatrix} y_0 \\ y_1 \\ y_2 \\ \vdots \\ y_S \end{bmatrix}, \quad \mathbf{u} = \begin{bmatrix} u_0 \\ u_1 \\ u_2 \\ \vdots \\ u_S \end{bmatrix}, \quad G = \begin{bmatrix} g_0 & 0 & 0 & \dots & 0 \\ g_1 & g_0 & 0 & \dots & 0 \\ g_2 & g_1 & g_0 & \dots & 0 \\ \vdots & \vdots & \vdots & \ddots & \vdots \\ g_S & g_{S-1} & \dots & \dots & g_0 \end{bmatrix},$$

being G a Toeplitz matrix whose elements are given by the previously introduced impulse response sequence g. As can be seen, the dimensions of G vary according to the length of the input and the output vector.

In this work, we consider the problem of finding an estimation of the input vector, say $\hat{\mathbf{u}}$, from a given an observation vector $\mathbf{y}$ and the Toeplitz matrix G. As we will see in the coming subsections, there are a few methods that can be used in this regard.

2.1. Direct inversion

We start a small review of methods to solve our problem by introducing the simplest method to perform numerical deconvolution in a non-parametric fashion, which is known as direct inversion and leads us to solve algebraically a system of equations derived from Eq. (2) as

$$\hat{\mathbf{u}} = G^{-1}\mathbf{y},$$

which is possible as long as G has an inverse. However, this method has poor performance because G can be ill-conditioned, showing high sensitivity with respect to changes in $\mathbf{y}$, i.e., it can generate a significant variability of the estimate with minor changes in the measurements.

2.2. Least squares with regularization approach

Alternatively, one can find $\hat{u}$ so that the sum of the squared of the residuals

$$r = \mathbf{y} - G\mathbf{u}$$

are minimized, i.e.,

$$\hat{\mathbf{u}} = \arg\min_{\mathbf{u}} (\mathbf{y} - G\mathbf{u})^\top (\mathbf{y} - G\mathbf{u}).$$

This is a well-known optimization problem and its minimizer,

$$\hat{\mathbf{u}} = (G^\top G)^{-1} G\mathbf{y}, \tag{3}$$

is derived in many books and articles such as [16]. However, the approach is not without its limitations, specially when $G^\top G$ is near-singular.

To relieve computation issues when applying least-squares, works such as [19] propose shifting the diagonal of $(G^\top G)$ by adding and extra term $\lambda_{\text{reg}} I$, where I is an unit matrix of the corresponding size, as

$$\hat{\mathbf{u}} = (G^\top G + \lambda_{\text{reg}} I)^{-1} G^\top \hat{\mathbf{y}}.$$

Here, $\lambda_{\text{reg}} > 0$ is the so-called ridge parameter, and enters as a regularization factor that alleviates numerical issues. This solution also corresponds to the minimizer of the following optimization problem

$$\hat{\mathbf{u}} = \arg\min_{\mathbf{u}} (\mathbf{y} - G\mathbf{u})^\top (\mathbf{y} - G\mathbf{u}) + \lambda_{\text{reg}} (\mathbf{u}^\top \mathbf{u} - c),$$

i.e., λ_{reg} can be seen as a Lagrange multiplier that penalizes the violation of the constraint $\mathbf{u}^\top \mathbf{u} = c$, where $c > 0$. Therefore, tuning λ_{reg} promotes a regularization of the norm of the estimated input via the cost function.

More advanced versions of this method have been proposed in the literature, e.g., in [14], where the input sequence is estimated as

$$\hat{\mathbf{u}} = \arg\min_{\mathbf{u}} \left((G\mathbf{u} - \mathbf{y})^\top \Sigma_{\text{v}}^{-1} (G\mathbf{u} - \mathbf{y}) + \lambda_{\text{reg}} \mathbf{u} \Sigma_{\text{u}}^{-1} \mathbf{u} \right), \tag{4}$$

[1] The assumption that both signals are zero for $k < 0$ is based on the causality principle, wherein the output at any given time is influenced only by current and past inputs, not future ones. However, this assumption could be relaxed since our method does not inherently restrict its application to solely causal systems.

where, once more, λ_{reg} can be arbitrarily changed to obtain a trade-off between fidelity to the data and *roughness* of the input sequence estimate. In this version, Σ_{v} and Σ_{u} can be interpreted as variances of the output error and the input estimate, respectively, with the input sequence modeled as an integrated random walk model. From this viewpoint, these variances represent the prior knowledge of the output and input, which allows generating confidence intervals on the results obtained.

2.3. Numerical deconvolution based on orthogonal polynomials

This is a parametric approach that decomposes the input as

$$\underbrace{\begin{bmatrix} \hat{u}_0 \\ \hat{u}_1 \\ \vdots \\ \hat{u}_S \end{bmatrix}}_{\hat{\mathbf{u}}} = \underbrace{\begin{bmatrix} u_0^{[1]} & u_0^{[2]} & \dots & u_0^{[n]} \\ u_1^{[1]} & u_1^{[2]} & \dots & u_1^{[n]} \\ \vdots & \vdots & \ddots & \vdots \\ u_S^{[1]} & u_S^{[2]} & \dots & u_S^{[n]} \end{bmatrix}}_{U} \underbrace{\begin{bmatrix} a_1 \\ a_2 \\ \vdots \\ a_n \end{bmatrix}}_{a}, \tag{5}$$

where a is a vector containing n scalar coefficients. Given the duality between discrete-time sequences and vectors, this means that

$$\hat{u}_k = \sum_{i=1}^{n} a_i u_k^{[i]}, \quad \forall k \in \{0, 1, ..., S\}.$$

That is, the deconvolved input becomes a linear combination of the columns of matrix U, where $u^{[i]}$ represents the i-th column of matrix U, i.e., $U = [u^{[1]}\ u^{[2]}\ \dots\ u^{[n]}]$, and $u_k^{[i]}$ corresponds to its value at time instant (and row) k.

For reasons that will become apparent shortly, we are specifically looking for vectors $u^{[i]}$ that stem from a polynomial. In our discrete-time setting, this means that

$$u^{[i]} = M_i b^{[i]}, \tag{6}$$

where $b^{[i]} = [b_{i,1}, b_{i,2}, \dots, b_{i,i}]^\top$ is a vector containing i scalar coefficients and

$$M_i = [m^{[1]}\ m^{[2]}\ \dots\ m^{[i]}], \tag{7}$$

is a matrix containing i vectors of the form $m^{[i]} = [m_0^{[i]}, m_1^{[i]}, \cdots, m_S^{[i]}]^\top$, where $m_k^{[i]} = k^i$. Note that these vectors are *monomials* and therefore one can think of matrix M as a monomial matrix. In particular, $m^{[i]}$ is simply defined as the sequence containing the component-wise i-th power of the discrete-time index k. In a continuous time setting, this corresponds to the i-th power of the corresponding samples of the time vector, which explains why signals generating vectors as that written as Eq. (6) are *polynomials*.

Again, this means that

$$u_k^{[i]} = \sum_{j=1}^{i} b_j^{[i]} m_k^{[j]} = \sum_{j=1}^{i} b_j^{[i]} k^j, \quad \forall k \in \{0, 1, ..., S\}.$$

Likewise, the estimated output vector, say $\hat{\mathbf{y}} = [\hat{y}_0, \hat{y}_1, ..., \hat{y}_S]^\top$, is given by $\hat{\mathbf{y}} = GUa$, and, therefore,

$$\hat{y}_k = \sum_{t=0}^{k} g_{k-t} \sum_{i=1}^{n} a_i u_t^{[i]} = \sum_{i=1}^{n} a_i \underbrace{\sum_{t=0}^{k} g_{k-t} u_t^{[i]}}_{f_k^{[i]}}, \quad \forall k \in \{0, 1, ..., S\},$$

where $f_k^{[i]}$ denotes the k-th element of the sequence stemming from the linear transformation that is performed by the system on input vector $u^{[i]}$.

Writing the input estimate following equations (5)-(7) offers advantages from a numerical viewpoint if the data-fitting process in a least-squares sense is performed using a set of orthogonal polynomial functions. This is precisely what was proposed by Cutler in [11], who adapted a well-known process for data fitting taken from [16] to the specific case of the input deconvolution of a linear system. In particular, Cutler customized the Gram-Schmidt orthogonalization method to find coefficients vector a that minimizes the following objective function for any given polynomial order n:

$$J(a) = \sum_{k=0}^{S} \left(y_k - \sum_{i=1}^{n} a_i f_k^{[i]} \right)^2 = (\mathbf{y} - GUa)^\top (\mathbf{y} - GUa). \tag{8}$$

The core of this approach is given in Algorithm 1 for a discrete-time linear system and works as follows[2]: input sequences $u^{[i]}$ for $i = 1, 2, ..., n$ (the columns of the previously introduced matrix U) are generated such that they result in orthogonal outputs, i.e.,

$$(y^{[i]})^\top y^{[j]} = 0, \quad \forall i, j \in \{1, 2, \dots, n\}, \ i \neq j, \tag{9}$$

where $y^{[i]} = Gu^{[i]}$. Then, the estimated input of the system can be described as a weighted sum of the input vectors, i.e., $\hat{\mathbf{u}} = \sum_i a_i u^{[i]}$, where a_i is a coefficient computed from the projection of the output data vector $\mathbf{y}$ onto $y^{[i]}$.

In a nutshell, the method starts calculating the step response of the system and computes the projection of the measured output onto it (again, recall that sampled signals and vectors work analogously in this context), yielding coefficient a_1. The next input polynomial is defined by multiplying the previous one by the discrete-time index and subtracting its projections of its output onto the previously computed output polynomials. For example, the second polynomial becomes a ramp minus a step weighted by $b_{1,1}$, which is calculated to guarantee that the orthogonality at the output with the previous output polynomial. In this way a_2 can be computed as the projection of the observed output onto the output corresponding to the second input polynomial. This basic process is iterated until the predefined polynomial order n is attained. Also, note that it is possible to set a different stopping criterion. For example, one could keep adding terms until a threshold on the value attained by the residual mean square at the output generated by the current estimate is met, or until an indicator as the Akaike information criterion recommends to do so [3,6].

Finally, we conclude this subsection by providing an algebraic expression of the solution of Cutler's approach, which was not derived in his manuscript despite its evident advantages to keep the notation simple. In particular, it is possible to compute the vector of coefficients a considering (8), yielding $a^* = \arg\min_a (\mathbf{y} - GUa)^\top (\mathbf{y} - GUa)$. By defining $G' = GU$, we can obtain an analogous solution to that of (3), i.e.,

$$a = (G'^{\mathrm{T}} G')^{-1} G' \mathbf{y} = (U^\top G^\top G U)^{-1} G U \mathbf{y}. \tag{10}$$

To apply the solution of Equation (10), it is necessary to obtain first the set of vectors U that generate orthogonal outputs. This can be done, for example, employing the variation of the Gram-Schmidt method that is given in the loop of Algorithm 1.

Algorithm 1: Numerical deconvolution based on orthogonal output sequences for discrete-time linear systems.

Define parameter n, initialize $u^{[1]} = [1, 1, \cdots, 1]^\top \in \mathbb{R}^{(S+1)\times 1}$, and set $T = \mathrm{diag}(m^{[1]}) = \mathrm{diag}([0, 1, 2, \cdots, S])$. Then,

for $i = 1, \dots, n$ **do**

$u^{[i+1]} = Tu^{[i]} - \sum_{k=1}^{i} b_{i,k} u^{[k]}$, with $b_{i,k} = \frac{u^{[i]\top} T^\top G^\top G u^{[k]}}{u^{[k]\top} G^\top G u^{[k]}}$;

end

Result: Deconvolved input $\hat{\mathbf{u}} = \sum_{i=1}^{n} a_i^* u^{[i]}$, where $a_i^* = \frac{\mathbf{y}^\top G u^{[i]}}{u^{[i]\top} G^\top G u^{[i]}}$.

3. Constrained numerical deconvolution based on orthogonal polynomials

While Cutler's method solves numerical issues regarding the computation of the input estimate in a parametric form, it has some downsides. For example, the estimates generated might not have sense from a physical viewpoint, e.g., deconvolved signals might become negative at some points, which is not realistic in application fields such as pharmacokinetics, where magnitudes as concentration are required to be positive. Also, the resulting signals may exhibit strong fluctuations in some cases, specially at the end of their range when the effect of the deconvolved input is only partially visible on the output. This section presents several alternatives to relieve these issues or to fix them altogether by adapting some well known approaches to the current setup. By doing this, we enhance the applicability of the original approach proposed by Cutler and provide means to compute realistic input estimates in a parametric and numerical fashion, also respecting an inherent feature of Cutler's original method, which is its reliance on the Gram-Schmidt orthogonalization process to derive orthogonal polynomials for each specific application rather than using conventional orthogonal polynomial families.

Given the previously mentioned issues, in this section we provide two alternatives. The first one is the introduction of a regularization term, which has the potential to solve minor constraint violations. The second mechanism is based on the introduction of the constraints in the cost function optimized using Lagrangian multipliers. In developing these alternatives, we aimed to preserve the foundational aspects of Cutler's method, particularly its emphasis on the Gram-Schmidt process for orthogonalization. This adherence not only ensures compatibility with the original method but also maximizes the orthogonality and efficiency of the derived polynomials. As will be seen, the two algorithms proposed respect the essence of the original Cutler's method, enhancing its applicability to situations where constraints on signal values are significant.

[2] To simplify the introduction of the method, we assume that the output of the system can be observed at each sampling time. This is done without loss of generality because it is straightforward to extend the method for the case of sparse measurements.

3.1. Relieving constraint satisfaction via regularization approach

First, we modify the method by providing it with a regularization term similarly to Eq. (4). That is, the objective function we want to minimize is the following:

$$J_{\text{reg}}(a) = \sum_{k=0}^{S} \left(y_k - \sum_{i=1}^{n} a_i f_k^{[i]} \right)^2 + \sum_{i=1}^{n} \zeta(i) a_i^2,$$

where $\zeta(i) > 0$ is a function of parameter i that regularizes coefficient a_i. Note that this function allows penalizing more those coefficients associated with higher degrees polynomials. This way, it is possible to avoid extreme input estimates, so that vector $\hat{\mathbf{u}}$ becomes more plausible. Following similar steps as the original Cutler's method, we will calculate coefficients a_j, for all $j \in \{1, ..., n\}$, by computing partial derivatives $\partial J_{\text{reg}}(a)/\partial a_j$, i.e.,

$$\frac{\partial J_{\text{reg}}(a)}{\partial a_j} = 2 \sum_{k=0}^{S} \left(y_k - \sum_{i=1}^{n} a_i f_k^{[i]} \right) f_k^{[j]} + 2\zeta(i) a_i. \tag{11}$$

Again, consider that (9) holds, then $\sum_{k=0}^{S} f_k^{[i]} f_k^{[j]} = 0$ for all $i \neq j$. Given this and equating (11) to zero, we have that

$$-\sum_{k=0}^{S} y_k f_k^{[j]} + a_j^* \sum_{k=0}^{S} f_k^{[j]} f_k^{[j]} + a_j^* \zeta(j) = 0.$$

Finally, isolating coefficients a_j^* and using a matrix notation, we obtain

$$a_j^* = \frac{\sum_{k=0}^{S} y_k f_k^{[j]}}{\sum_{k=0}^{S} (f_k^{[j]})^2 + \zeta(j)} = \frac{\mathbf{y}^\top G u^{[j]}}{u^{[j]\top} G^\top G u^{[j]} + \zeta(j)}. \tag{12}$$

The extended Cutler's method with regularization factor is finally summarized in Algorithm 2.

Finally, we generalize these results in an algebraic form:

$$a = (U^\top G^\top Q G U + Z)^{-1} Q G U \mathbf{y}$$

where Q and Z are weighting matrices that can be exploited to obtain confidence intervals regarding the output and its corresponding deconvolved input (recall [14]). Note that the equivalence with Equation (12) is attained if $Z = \text{diag}(\zeta_i)$ and Q is equal to the unit matrix of the corresponding size. Also, the weighting matrix penalizing the output can include zero rows so as to model the absence of measurements —a very frequent situation in the biomedical context—, yielding a series of coincidence points to drive the calculation of the coefficients.

Algorithm 2: Numerical deconvolution based on orthogonal output sequences for discrete-time linear systems with regularization term.

Define parameters n and function $\zeta(\cdot)$, initialize $u^{[1]} = \mathbf{1}_{S+1} = [1, 1, \cdots, 1]^\top$, and set $T = \text{diag}(m^{[1]}) = \text{diag}([0, 1, \cdots, S])$. Then,

for $i = 1, \ldots, n$ **do**

$u^{[i+1]} = T u^{[i]} - \sum_{k=1}^{i} b_{i,k} u^{[k]}$, with $b_{i,k} = \frac{u^{[i]\top} T^\top G^\top G u^{[k]}}{u^{[k]\top} G^\top G u^{[k]}}$.

end

Result: Deconv. input $\hat{\mathbf{u}} = \sum_{i=1}^{n} a_i^* u^{[i]}$, with $a_i^* = \frac{\mathbf{y}^\top G u^{[i]}}{u^{[i]\top} G^\top G u^{[i]} + \zeta(i)}$.

3.2. Enforcing constraint satisfaction via Lagrangian multipliers

The regularization method introduced in the previous subsection can relieve issues related to extreme realization of the estimate. However, it does not guarantee that the values of the deconvolved input vector $\hat{\mathbf{u}} = [\hat{u}_k]_{k=0}^{S}$ or estimated output $\hat{\mathbf{y}} = [\hat{y}_k]_{k=0}^{S}$ are realistic. For example, we may require them to contain only nonnegative numbers. In order to address this type of conditions, we will assume that coefficients vector a must satisfy the following inequalities for any given n:

$$\begin{aligned} \hat{u}_k &= \sum_{i=1}^{n} a_i u_k^{[i]} \geq \gamma^{\text{u}}, \\ \hat{y}_k &= \sum_{i=1}^{n} a_i f_k^{[i]} \geq \gamma^{\text{y}}, \\ &\forall k \in \{0, 1, ..., S\}, \end{aligned} \tag{13}$$

where γ^{u} and γ^{y} can be freely chosen. In what follows, we will consider Lagrangian-based methods together with Cutler's algorithm to perform a constrained deconvolution. Particularly, we will optimize objective function (8) subject to (13) using a dual-ascent algorithm [5].

Let us use $\tilde{a}_i = -a_i$, and similarly $\tilde{a} = -a = [-a_i]_{i=1}^n$. Also, note that the new problem we address can be formulated as

$$\min_{\tilde{a}} \sum_{k=0}^{S} \left(y_k + \sum_{i=1}^{n} \tilde{a}_i f_k^{[i]} \right)^2 = (\mathbf{y} + GU\tilde{a})^\top (\mathbf{y} - GU\tilde{a}) \tag{14a}$$

$$\text{s.t.} \quad \underbrace{\begin{bmatrix} U \\ GU \end{bmatrix}}_{H} \tilde{a} \leq \underbrace{\begin{bmatrix} -\gamma^{\mathrm{u}} \mathbf{1}_{S+1} \\ -\gamma^{\mathrm{y}} \mathbf{1}_{S+1} \end{bmatrix}}_{-\boldsymbol{\gamma}}, \tag{14b}$$

where $\mathbf{1}_t$ denotes the all-ones vector of dimensions $t \times 1$, for any natural number t. Likewise, let us use $\mathbf{0}_t$ to denote the all-zeros vector of corresponding dimensions, and let us denote the i-th column of matrix H as $h^{[i]}$, i.e., $H = [h^{[1]}, h^{[2]}, ..., h^{[n]}]$. By forming the Lagrangian function of (14), the associated dual problem is given by

$$\max_{\lambda} \min_{\tilde{a}} \ \tilde{\mathcal{L}}_n(\tilde{a}, \lambda) = \sum_{k=0}^{S} \left(y_k + \sum_{i=1}^{n} \tilde{a}_i f_k^{[i]} \right)^2 + \lambda^\top \sum_{i=1}^{n} h^{[i]} \tilde{a}_i,$$

where $\lambda \geq \mathbf{0}_{2(S+1)}$ is the vector of multipliers associated with (14b). Considering the above, problem (14) will be addressed by implementing the dual gradient ascent method in Algorithm 3. Note that the latter presents an iterative procedure where both Lagrange multipliers and Cutler's coefficients vector a are repeatedly updated until convergence. In this regard, an explicit expression of coefficients a_i for all $i \in \{1, 2, ..., n\}$ is derived following similar steps as in Cutler's original method. In particular, equating the partial derivative $\partial \tilde{\mathcal{L}}_n(\tilde{a}, \lambda)/\partial \tilde{a}_j$ to zero for any $j \in \{1, 2, ..., n\}$, we obtain

$$\sum_{k=0}^{S} \left(y_k + \sum_{i=1}^{n} \tilde{a}_i f_k^{[i]} \right) f_k^{[j]} \ + \ 0.5\lambda^\top h^{[j]} = 0.$$

If $\sum_{k=0}^{S} f_k^{[i]} f_k^{[j]} = 0$ for all $i \neq j$, then,

$$\sum_{k=0}^{S} y_k f_k^{[j]} + \tilde{a}_j^* \sum_{k=0}^{S} f_k^{[j]} f_k^{[j]} + 0.5\lambda^\top h^{[j]} = 0. \tag{15}$$

From (15), it is straightforward to derive an explicit expression for coefficient $a_j^* = -\tilde{a}_j^*$ as a function of the Lagrange multipliers, i.e.,

$$a_j^* = \frac{\sum_{k=0}^{S} y_k f_k^{[j]} + 0.5\lambda^\top h^{[j]}}{\sum_{k=0}^{S} f_k^{[j]} f_k^{[j]}} = \frac{\mathbf{y}^\top G u^{[j]} + 0.5\lambda^\top h^{[j]}}{u^{[j]\top} G^\top G u^{[j]}}.$$

Algorithm 3: Cutler Method with Lagrangian Multipliers.

Let superscript p be the iteration index, $\alpha > 0$ the step size for the multipliers update, initialize $\lambda^0 \geq \mathbf{0}_{2(S+1)}$, and set parameters n and $\boldsymbol{\gamma}$. Then, starting from $p = 0$, consider the following steps:

1) Run the original Cutler's method to find $u^{[i]}$ for all $i \in \{1, 2, ..., n\}$.

2) Compute coefficients a_i:

for $i \in \{1, 2, ..., n\}$ **do**

$$a_i^p = \frac{\mathbf{y}^\top G u^{[i]} + 0.5\lambda^{p-1\top} h^{[i]}}{u^{[i]\top} G^\top G u^{[i]}}.$$

3) Update $\lambda^p = \max\left\{ \lambda^{p-1} + \alpha(\boldsymbol{\gamma} - H a^p), \mathbf{0}_{2(M+1)} \right\}$, where $a^p = [a_i^p]_{i=1}^n$.

4) Define $a^* = [a_i^*]_{i=1}^n = a^p$, set $p \leftarrow p + 1$, and go to step 2) until convergence is reached.

Result: Deconvolved input $\hat{\mathbf{u}} = \sum_{i=1}^{n} a_i^* u^{[i]}$.

4. Case studies

In this section, we demonstrate the effectiveness of our proposed deconvolution method in two different applications, namely, the estimation of COVID-19 contagion curves and the characterization of the absorption process of mavoglurant. Keep in mind that these examples do not intend to be exhaustive applications of the method, but illustrative examples of how our proposal can help overcome some of the issues that appear when applying the original Cutler method or some other well-known approaches. Finally,

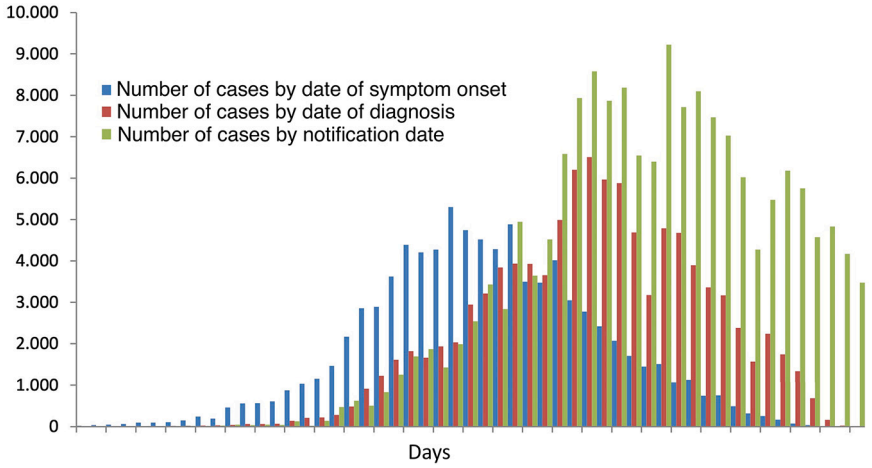

Fig. 1. Official data published by Spanish health authorities. Blue data represent reported symptom onset; red data represent daily cases by diagnose date; green data stand for daily notification data.

to analyze the performance of our extended Cutler's method, we focus on a quantitative performance measure — the sum of squared residuals (SSR)— and a qualitative one —the existence of constraint violations, which can be appreciated by visual inspection.[3]

4.1. Covid-19 contagion curves

The stochastic time-delay existing between the exposure to the virus and its potential detection complicates the reconstruction of the contagion curves. One way to deal with this issue, is to apply deconvolution methods as was done, e.g., in [18] to reconstruct the incidence curves for the 1918 influenza epidemic.

One simple way to test this approach is to use the abundant data from the COVID-19 pandemic. To this end, let us go back to the early stages of the pandemic, so that we can show what the application of the considered methods would have yielded based on the early characterization of the contagion dynamics. In particular, several works estimated the disease incubation period by using empirical data from China. For example, in February 2020, [4] and [24] reported respectively a mean incubation period of 6.4 days and 5.6 days. In addition, [41] estimated a median incubation time of 6.7 days, and a interval time of 4.5 days between the symptoms onset and the hospital visit, with a median time of 2.1 days between the visit to the hospital until the positive confirmation. See also [22], which estimated a median incubation period of 5.1 days, with fewer than 2.5% cases displaying symptoms within the first 2.2 days after exposure, and symptom onset occurring within 11.5 days for 97.5% of them. Note that the reported estimates were generally in line with those of other known human coronaviruses, including SARS [8] and MERS [44]. Likewise, more recent works such as [29,27] have also reported incubation periods of about 6 days for different variants of COVID-19.

With these descriptions in mind, let us consider now the events that occurred in March of that year in Spain, for it is well-known that Spain was one of the most affected countries during the first wave of the COVID-19 pandemic, in part due to its initial lack of measures despite that neighboring countries like Italy were already suffering the pandemic. Therefore, let us use the same data released by the Spanish health authorities on the number of COVID-19 cases over time to estimate the contagion curves. In particular, Fig. 1 displays the official number of COVID-19 infections according to the date of diagnosis and date of symptom onset [1]. This figure is convenient because it provides information of the disease at different stages, but also it allows the estimation of the actual contagion curve from the symptom onset curve base on the Chinese studies.

To obtain the contagion curve, we apply our deconvolution method, and the resulting estimations are depicted in Fig. 2. In this regard, we have considered $n = 10$, $\gamma^{\mathrm{u}} = 0$, $\gamma^{\mathrm{y}} = 0$, and $\zeta(i) = 0.25i^2$ for all $i = 1, 2, ..., 10$.[4] On the left column of Fig. 2, the estimations provided by the considered methods are shown. As can be seen, Cutler's original method fails by exhibiting a very unrealistic behavior by the end, although this issue does not affect the reconstructed output for the period that has been evaluated; the direct inversion method is not able to deal with the problem and encounters numerical issues that deprive the resulting estimate of any physical sense; also, non-negative least squares provide a very unlikely trajectory for the deconvolved signal, although the corresponding estimate for the output, which is shown on the right, correctly follows the reference output; the incorporation of a ridge-factor, has

[3] The MATLAB prototype code used for the experiments in this manuscript is available upon direct request to the authors. While the algorithms presented in the article are straightforward and can be readily implemented, the code developed is tailored for our specific experiments. Interested researchers may contact the corresponding author for access and further clarifications.

[4] Parameters γ_{u} and γ_{y}, which determine the constraints, were chosen so that the corresponding variables have a realistic physical meaning. For example, we use $\gamma_{\mathrm{u}} = \gamma_{\mathrm{y}} = 0$ since both u and y represent numbers of people, and therefore cannot be negative. In addition, degree n was set so that the original Cutler's method provided relatively accurate output estimations. Finally, parameter ζ, which weights the regularization term, was set so as to observe some differences between the original Cutler's method and its regularized variant.

Table 1
SSR of the assessed methods for the Covid-19 case study.

Method	SSR
Cutler	2.231688e+06
Direct Inversion	2.573134e+178
Non negative LS	8.774296e+05
Cutler + RF	2.683020e+06
Cutler + LM	2.460620e+06
Cutler + RF + LM	2.464768e+06

Table 2
Coefficients of assessed parametric methods for the Covid-19 case study.

Coefficient	Cutler	Cutler + RF	Cutler + LM	Cutler + RF + LM
a_1	1.839e+03	1.829e+03	1.855e+03	1.846e+03
a_2	-1.753e+01	-1.626e+01	-1.573e+01	-1.565e+01
a_3	-8.560e+00	-8.688e+00	-8.388e+00	-8.379e+00
a_4	1.590e-01	1.636e-01	1.707e-01	1.711e-01
a_5	2.853e-02	2.830e-02	2.923e-02	2.927e-02
a_6	-1.071e-03	-1.028e-03	-1.069e-03	-1.070e-03
a_7	-6.347e-05	-6.291e-05	-6.560e-05	-6.570e-05
a_8	5.834e-06	4.807e-06	5.467e-06	5.425e-06
a_9	4.959e-08	1.607e-07	7.313e-08	7.348e-08
a_{10}	-2.146e-08	-1.751e-08	-1.103e-08	-1.091e-08

difficulties to correct the issues with Cutler's method; finally, the use of the Lagrangian multipliers allows reconstructing plausible estimates, providing superior results when the ridge factor is not employed.

Finally, Tables 1 and 2 respectively provide the sum of squared residuals (SSR) of each method and the coefficients corresponding to Cutler's original method and the proposed variations. As can be seen, relying only on SSR can be misguiding, for its superior performance is attained using a very unrealistic deconvolved signal. In other words, it is worth sacrificing some performance in terms of SSR for the sake of realism. Also, Table 2 show that the proposed methods tend to have greater impact on higher order coefficients, which makes sense since high-powered polynomials are more likely to generate larger deviations in the deconvolved signals.

4.2. Mavoglurant

Mavoglurant is an experimental drug candidate to mitigate the fragile X syndrome, which is related to autism and mental retardation. Its main disposition characteristics appear summarized in Table 3; the reader is referred to [45] and the references therein for an extensive description of the dataset, which comprised two studies, one measuring the response from a single 10-min IV infusion of the drug in 120 healthy subjects to characterize its pharmacokinetics and another focused on studying different release formulations under fasted and fed conditions.

The best characterization of the pharmacokinetics was provided by the following two state linear time-invariant model:

$$\begin{aligned} \frac{dA_1}{dt} &= I(t) - A_1(c_{10} + c_{12}) + A_2 c_{21} \\ \frac{dA_2}{dt} &= A_1 c_{12} - A_2 c_{21} \end{aligned} \tag{16}$$

where A_1 and A_2 respectively stand for the amount of drug (in mg) in the central peripheral compartments, measured in miligrams; c_{10}, c_{12} and c_{21} are first-order rate constants in h^{-1} related to drug elimination and inter-compartmental transfers, respectively. Finally, $I(t)$ represents the drug input in the central compartment. The relationship between the parameters in Equation (16) and those in Table 3 is given by

$$c_{12} = Q/V_c,$$
$$c_{21} = Q/V_p,$$
$$c_{10} = CL/V_c.$$

These equations have been programmed in Matlab so that the proposed method could be tested. Here, it is interesting that the pooled clinical studies found difficulties in characterizing the absorption process, which showed puzzling complexity as it exhibited several peaks, making it impossible to find a suitable linear model. As a consequence, the approach followed in [45] was to use a sum of three inverse Gaussian functions to describe the outcome of an oral dose. In this work, we exploit what is known about the model to find suitable input sequences that explain the experimental behavior found in oral absorption data.

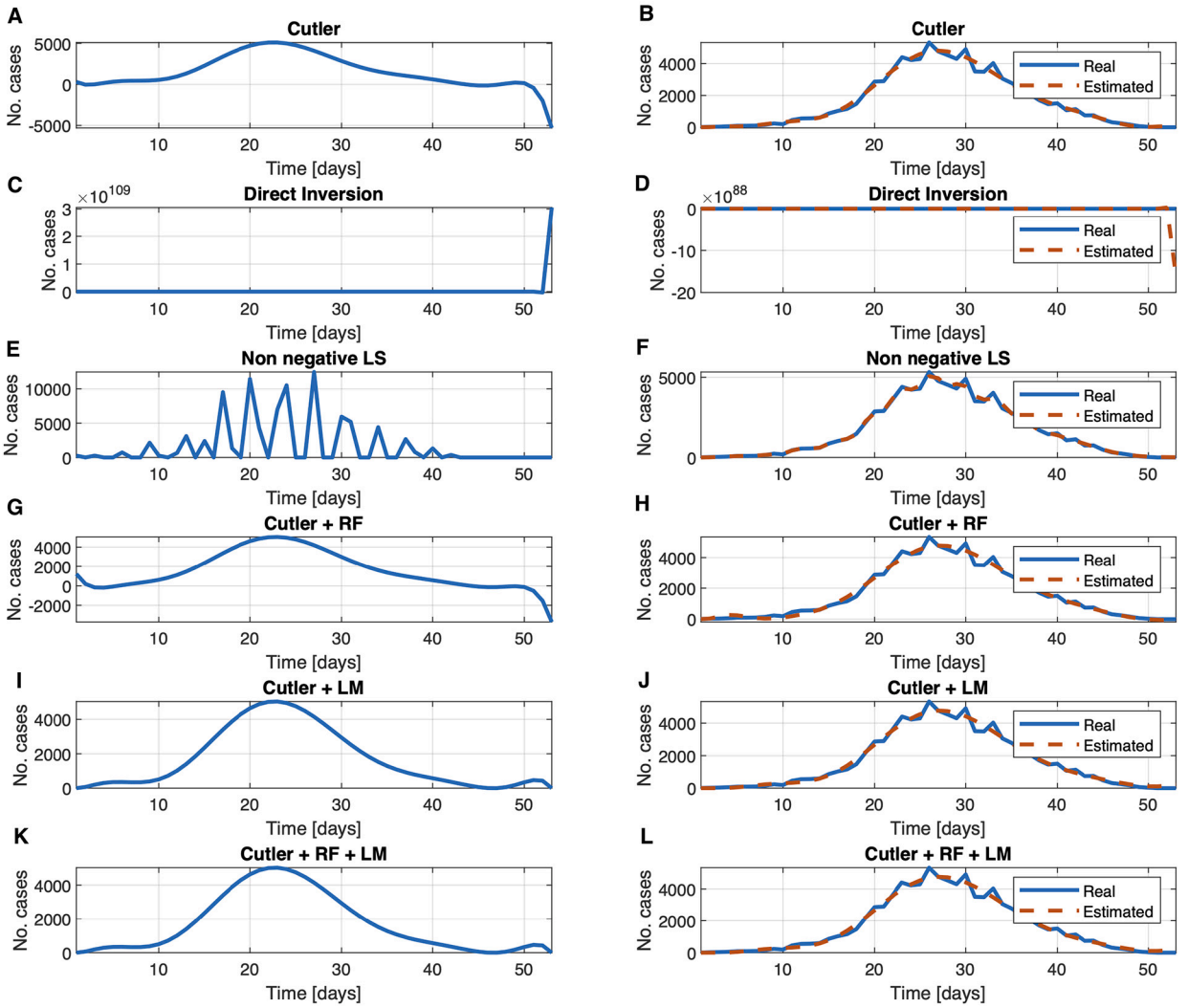

Fig. 2. Comparative analysis of deconvolution methods on contagion curve estimation during the first COVID-19 wave in Spain. Panels on the left column display the contagion estimates and those on the right column show the corresponding output estimates for each method (dashed red line) highlighting the deviation from the reference output (continuous blue line): (A, B) Cutler's Original Method; (C, D) Direct Inversion; (E, F) Non-negative least squares; (G, H) Cutler with ridge factor; (I, J) Cutler with Lagrangian multipliers; and (K, L) Cutler with ridge factor and Lagrangian multipliers.

Table 3
Estimates of Mavoglurant Disposition Parameters [45].

Parameter	Symbol	Units	Mean	%RSE
Volume of distribution of central compartment	V_c	l	58.7	3.75
Body weight covariate	θ_{BW,V_c}	kg	0.543	26.1
Volume of distribution of peripherical compartment	V_p	l	113	4.48
Body weight covariate	θ_{BW,V_p}	kg	1.13	12.1
Plasma clearance	CL	l/h	29.3	2.48
Inter-compartmental clearance	Q	l/h	24.8	3.72

Fig. 3 shows the reconstruction of the input for the methods assessed, which corresponds to the output of the absorption process. These results have been obtained using parameters $n = 25$, $\gamma^u = 0$, $\gamma^y = 0$, and $\zeta(i) = 2.5i^2$ for all $i = 1, 2, ..., 25$. Here, the previously mentioned multiple peak issue can be clearly seen. Also, Cutler's original method once more returns a deconvolved input with some negative parts, although the issue is less severe compared with the previous case study. Again, this issue can be corrected when using Lagrange multipliers in the estimation so that this constraint can be taken into account. As for the comparison in terms of SSR, Table 4 indicates that the best result is obtained by Direct Inversion, but then again one must note that this superior result is

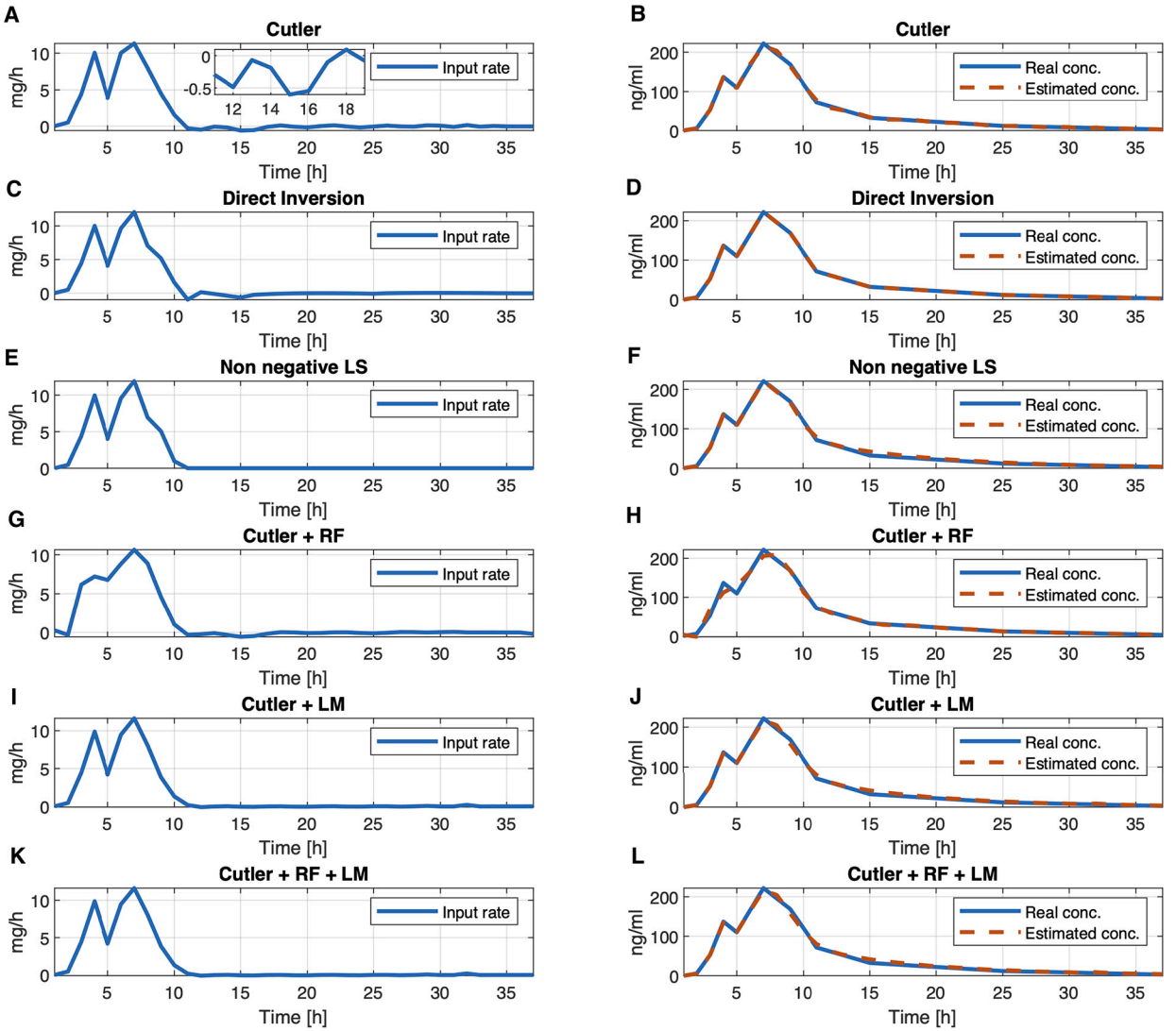

Fig. 3. Comparative analysis of deconvolution methods on the outcome of the absorption process on a subject after an oral dose of Mavoglurant. Panels on the left column display the contagion estimates and those on the right column show the corresponding output estimates for each method (dashed red line) highlighting the deviation from the reference output (continuous blue line): (A, B) Cutler's Original Method; (C, D) Direct Inversion; (E, F) Non-negative least squares; (G, H) Cutler with ridge factor; (I, J) Cutler with Lagrangian multipliers; and (K, L) Cutler with ridge factor and Lagrangian multipliers.

Table 4
SSR of the assessed methods for mavoglurant case study.

Method	SSR
Cutler	2.356918e+02
Direct Inversion	3.568215e-27
Non negative LS	4.329964e+02
Cutler + RF	1.862009e+03
Cutler + LM	6.327929e+02
Cutler + RF + LM	6.327519e+02

obtained with an unrealistic evolution of the deconvolved signal, which becomes negative at some points. Hence, it is clear that it is preferable to attain a slightly worse SSR if a more plausible signal is obtained. Finally, Table 5 shows the multiple coefficients of the parametric methods for this particular case. The growth in the number of coefficients of this case study is due to the peaks of the signal, which cannot be properly represented with lower-ordered polynomials. Again, the larger relative changes in the coefficient value appear in the coefficients with the highest order for the previously explained reasons.

Table 5
Coefficients of assessed parametric methods for the Mavoglurant case study.

Coefficient	Cutler	Cutler + RF	Cutler + LM	Cutler + RF + LM
a_1	1.394e+00	1.394e+00	1.442e+00	1.442e+00
a_2	-1.795e-01	-1.794e-01	-1.792e-01	-1.792e-01
a_3	1.117e-02	1.117e-02	1.061e-02	1.061e-02
a_4	3.036e-04	3.035e-04	3.477e-04	3.477e-04
a_5	-1.572e-04	-1.572e-04	-1.526e-04	-1.526e-04
a_6	1.796e-05	1.795e-05	1.713e-05	1.712e-05
a_7	-8.987e-07	-8.971e-07	-8.961e-07	-8.961e-07
a_8	-4.112e-08	-4.139e-08	-3.256e-08	-3.256e-08
a_9	1.173e-08	1.177e-08	1.108e-08	1.108e-08
a_{10}	-8.819e-10	-8.870e-10	-9.270e-10	-9.270e-10
a_{11}	-1.807e-12	-1.091e-12	1.066e-11	1.067e-11
a_{12}	6.816e-12	6.713e-12	6.679e-12	6.679e-12
a_{13}	-6.069e-13	-5.926e-13	-7.098e-13	-7.098e-13
a_{14}	-1.994e-14	-2.202e-14	-1.630e-14	-1.629e-14
a_{15}	1.317e-14	1.348e-14	1.304e-14	1.304e-14
a_{16}	-1.972e-15	-2.019e-15	-2.004e-15	-2.004e-15
a_{17}	1.508e-16	1.594e-16	1.586e-16	1.586e-16
a_{18}	5.831e-19	-1.267e-18	-3.617e-19	-3.621e-19
a_{19}	-2.073e-18	-1.613e-18	-1.945e-18	-1.946e-18
a_{20}	3.714e-19	2.519e-19	3.966e-19	3.966e-19
a_{21}	-4.460e-20	-1.564e-20	-5.042e-20	-5.042e-20
a_{22}	4.802e-21	-6.404e-22	5.365e-21	5.365e-21
a_{23}	-6.007e-22	8.219e-23	-5.126e-22	-5.125e-22
a_{24}	7.985e-23	-1.513e-24	3.843e-23	3.842e-23
a_{25}	-8.056e-24	9.744e-26	-3.454e-24	-3.452e-24

5. Conclusion

In conclusion, this paper presents a significant improvement over Cutler's original deconvolution method by addressing its limitations in estimating realistic input parameters. The extended method deals with constraints using a ridge factor and Lagrangian multipliers, which are applied iteratively. This approach maintains the original algorithm's iterative projection-based nature, avoiding the need for optimization solvers to perform constrained optimization. Moreover, the presented approach can handle a variety of signals and data types effectively, for Cutler's algorithm is an all-purpose deconvolution technique, it inherently possesses a broad applicability to diverse types of signals. In this regard, the inclusion of the ridge factor and the Lagrangian multipliers in our extension does not restrict its versatility. Through two practical applications —the analysis of COVID-19 curves and the study of mavoglurant, an experimental drug— we have demonstrated the effectiveness of our proposed method. The results show that our extension exchanges performance regarding the sum of squared residuals compared to the original Cutler's method and other well known deconvolution techniques that perform an unconstrained optimization, but obtains instead physically plausible solutions, correcting the errors introduced by the alternative methods considered. Therefore, it becomes a more versatile tool for solving deconvolution problems in various scientific disciplines. Potential future explorations could focus on integrating more constraints or prior data to further enhance the deconvolution process, accommodating time-varying systems, and multi-dimensional problems.

CRediT authorship contribution statement

J.M. Maestre: Writing – review & editing, Writing – original draft, Visualization, Validation, Software, Methodology, Investigation, Conceptualization. **P. Chanfreut:** Writing – review & editing, Writing – original draft, Visualization, Validation, Software. **L. Aarons:** Writing – review & editing, Validation, Supervision, Resources, Formal analysis, Conceptualization.

Declaration of competing interest

The authors declare the following financial interests/personal relationships which may be considered as potential competing interests: J. M. Maestre reports financial support was provided by Spain Ministry of Science and Innovation (Project C3PO-R2D2, with reference PID2020-119476RB-I00 MCIN/AEI/10.13039/501100011033). If there are other authors, they declare that they have no known competing financial interests or personal relationships that could have appeared to influence the work reported in this paper.

Data availability

This manuscript utilizes two primary data sources: Covid data and mavoglurant data. The accessibility of these datasets is as follows:

- Covid Data: The Covid data employed in this study are publicly available. These data were sourced from [1], which is an openly accessible repository. This ensures transparency and reproducibility in our analysis of the Covid-related aspects of this study.
- Mavoglurant Data: These data were derived from a previous study conducted by one of the authors. Due to the proprietary nature of this research and previous confidentiality agreements, the detailed mavoglurant data cannot be shared openly. For further inquiries about the mavoglurant data, interested researchers can contact Stalicla, which is the current owner of the rights of this compound.

Acknowledgements

Financial support from the Spanish MCIN/AEI/10.13039/501100011033 Project C3PO-R2D2 under Grant PID2020-119476RB-I00 is gratefully acknowledged.

References

[1] Spanish Ministry of Health, Reports published during the health crisis, https://cnecovid.isciii.es/covid19/.
[2] Sadiq H. Abdulhussain, Basheera M. Mahmmod, Thar Baker, Dhiya Al-Jumeily, Fast and accurate computation of high-order Tchebichef polynomials, Concurr. Comput., Pract. Exp. 34 (27) (2022) e7311.
[3] H. Akaike, A new look at the statistical model identification, IEEE Trans. Autom. Control 19 (6) (1974) 716–723.
[4] J.A. Backer, D. Klinkenberg, J. Wallinga, Incubation period of 2019 novel coronavirus (2019-nCoV) infections among travellers from Wuhan, China, 20–28 January 2020, Euro Surveill. 25 (5) (2020).
[5] Stephen Boyd, Neal Parikh, Eric Chu, Borja Peleato, Jonathan Eckstein, et al., Distributed optimization and statistical learning via the alternating direction method of multipliers, Found. Trends Mach. Learn. 3 (1) (2011) 1–122.
[6] J.E. Cavanaugh, A.A. Neath, The Akaike information criterion: background, derivation, properties, application, interpretation, and refinements, Wiley Interdiscip. Rev.: Comput. Stat. 11 (3) (2019) e1460.
[7] M. Chadli, A. Akhenak, J. Ragot, D. Maquin, State and unknown input estimation for discrete time multiple model, J. Franklin Inst. 346 (6) (2009) 593–610.
[8] Moira Chan-Yeung, Rui-Heng Xu, SARS: epidemiology, Respirology 8 (2003) S9–S14.
[9] C. Cobelli, A. Mari, S. Del Prato, S. De Kreutzenberg, R. Nosadini, I. Jensen, Reconstructing the rate of appearance of subcutaneous insulin by deconvolution, Am. J. Physiol: Endocrinol. Metab. 253 (5) (1987) E584–E590.
[10] A. Cornelio, E. Loli Piccolomini, J.G. Nagy, Constrained numerical optimization methods for blind deconvolution, Numer. Algorithms 65 (1) (2014) 23–42.
[11] D.J. Cutler, Numerical deconvolution by least squares: use of polynomials to represent the input function, J. Pharmacokinet. Biopharm. 6 (3) (1978) 243–263.
[12] D.J. Cutler, Numerical deconvolution by least squares: use of prescribed input functions, J. Pharmacokinet. Biopharm. 6 (3) (1978) 227–241.
[13] Z. Dai, I.G. Rosen, C. Wang, N. Barnett, S.E. Luczak, Using drinking data and pharmacokinetic modeling to calibrate transport model and blind deconvolution based data analysis software for transdermal alcohol biosensors, Math. Biosci. Eng. 13 (5) (2016) 911.
[14] G. De Nicolao, G. Sparacino, C. Cobelli, Nonparametric input estimation in physiological systems: problems, methods, and case studies, Automatica 33 (5) (1997) 851–870.
[15] Antonio J. Durán, Exceptional Charlier and Hermite orthogonal polynomials, J. Approx. Theory 182 (2014) 29–58.
[16] G.E. Forsythe, Generation and use of orthogonal polynomials for data-fitting with a digital computer, J. Soc. Ind. Appl. Math. 5 (2) (1957) 74–88.
[17] S. Gillijns, B. De Moor, Unbiased minimum-variance input and state estimation for linear discrete-time systems, Automatica 43 (1) (2007) 111–116.
[18] Edward Goldstein, Jonathan Dushoff, Junling Ma, Joshua B. Plotkin, David JD Earn, Marc Lipsitch, Reconstructing influenza incidence by deconvolution of daily mortality time series, Proc. Natl. Acad. Sci. 106 (51) (2009) 21825–21829.
[19] Arthur E. Hoerl, Robert W. Kennard, Ridge regression: biased estimation for nonorthogonal problems, Technometrics 12 (1) (1970) 55–67.
[20] Yebin Im, Yongsoo Kim, A comprehensive overview of RNA deconvolution methods and their application, Mol. Cells 46 (2) (2023) 99.
[21] M. Kakhi, S. Suarez-Sharp, T. Shepard, J. Chittenden, Application of an NLME–stochastic deconvolution approach to level a IVIVC modeling, J. Pharm. Sci. 106 (7) (2017) 1905–1916.
[22] S.A. Lauer, K.H. Grantz, Q. Bi, F.K. Jones, Q. Zheng, H.R. Meredith, A.S. Azman, N.G. Reich, J. Lessler, The incubation period of coronavirus disease 2019 (Covid-19) from publicly reported confirmed cases: estimation and application, Ann. Intern. Med. (2020).
[23] Lei Li, Terence P. Speed, Parametric deconvolution of positive spike trains, Ann. Stat. 28 (5) (2000) 1279–1301.
[24] N.M. Linton, T. Kobayashi, Y. Yang, K. Hayashi, A.R. Akhmetzhanov, S. Jung, B. Yuan, R. Kinoshita, H. Nishiura, Incubation period and other epidemiological characteristics of 2019 novel coronavirus infections with right truncation: a statistical analysis of publicly available case data, J. Clin. Med. 9 (2) (2020) 538.
[25] Ying Ma, Xiang Zhou, Spatially informed cell-type deconvolution for spatial transcriptomics, Nat. Biotechnol. 40 (9) (2022) 1349–1359.
[26] B.M. Mahmmod, S.H. Abdulhussain, T. Suk, M. Alsabah, A. Hussain, Accelerated and improved stabilization for high order moments of Racah polynomials, IEEE Access 11 (2023) 110502–110521.
[27] Mattia Manica, Maria Litvinova, Alfredo De Bellis, Giorgio Guzzetta, Pamela Mancuso, Massimo Vicentini, Francesco Venturelli, Eufemia Bisaccia, Ana I. Bento, Piero Poletti, et al., Estimation of the incubation period and generation time of SARS-CoV-2 Alpha and Delta variants from contact tracing data, Epidemiol. Infect. 151 (2023) e5.
[28] Adam Melnyk, Lena Kozarov, Sebastian Wachsmann-Hogiu, A deconvolution approach to modelling surges in Covid-19 cases and deaths, Sci. Rep. 13 (1) (2023) 2361.
[29] Ke Men, Yihao Li, Xia Wang, Guangwei Zhang, Jingjing Hu, Yanyan Gao, Ashley Han, Wenbin Liu, Henry Han, Estimate the incubation period of coronavirus 2019 (Covid-19), Comput. Biol. Med. 158 (2023) 106794.
[30] Andrew C. Miller, Lauren A. Hannah, Joseph Futoma, Nicholas J. Foti, Emily B. Fox, Alexander D'Amour, Mark Sandler, Rif A. Saurous, Joseph A. Lewnard, Statistical deconvolution for inference of infection time series, Epidemiology (Cambridge, Mass.) 33 (4) (2022) 470.
[31] Shahin Mohammadi, Neta Zuckerman, Andrea Goldsmith, Ananth Grama, A critical survey of deconvolution methods for separating cell types in complex tissues, Proc. IEEE 105 (2) (2016) 340–366.
[32] Charles P. Neuman, Dave I. Schonbach, Discrete (Legendre) orthogonal polynomials–a survey, Int. J. Numer. Methods Eng. 8 (4) (1974) 743–770.
[33] K.E. Oerter, V. Guardabasso, D. Rodbard, Detection and characterization of peaks and estimation of instantaneous secretory rate for episodic pulsatile hormone secretion, Comput. Biomed. Res. 19 (2) (1986) 170–191.
[34] Sedki M. Riad, The deconvolution problem: an overview, Proc. IEEE 74 (1) (1986) 82–85.
[35] Xujia Shang, Pan Zhang, Liguo Han, Yuanyun Yang, Yixiu Zhou, Joint FWI of active source data and passive virtual source data reconstructed using an improved multidimensional deconvolution, IEEE Trans. Geosci. Remote Sens. 61 (2023) 1–14.
[36] G. Sparacino, C. Cobelli, A stochastic deconvolution method to reconstruct insulin secretion rate after a glucose stimulus, IEEE Trans. Biomed. Eng. 43 (5) (1996) 512–529.

[37] Karthik Ramakrishnan Sreenivasan, Martin Havlicek, Gopikrishna Deshpande, Nonparametric hemodynamic deconvolution of FMRI using homomorphic filtering, IEEE Trans. Med. Imaging 34 (5) (2014) 1155–1163.
[38] Jean-Luc Starck, Eric Pantin, Fionn Murtagh, Deconvolution in astronomy: a review, Publ. Astron. Soc. Pac. 114 (800) (2002) 1051.
[39] Andre K. Takahata, Everton Z. Nadalin, Rafael Ferrari, Leonardo Tomazeli Duarte, Ricardo Suyama, Renato R. Lopes, Joao M.T. Romano, Martin Tygel, Unsupervised processing of geophysical signals: a review of some key aspects of blind deconvolution and blind source separation, IEEE Signal Process. Mag. 29 (4) (2012) 27–35.
[40] E. Thiébaut, Optimization Issues in Blind Deconvolution Algorithms, Astronomical Data Analysis II, vol. 4847, SPIE, 2002, pp. 174–183.
[41] S. Tian, N. Hu, J. Lou, K. Chen, X. Kang, Z. Xiang, H. Chen, D. Wang, N. Liu, D. Liu, et al., Characteristics of Covid-19 infection in Beijing, J. Infect. (2020).
[42] P. Veng-Pedersen, An algorithm and computer program for deconvolution in linear pharmacokinetics, J. Pharmacokinet. Biopharm. 8 (5) (1980) 463–481.
[43] D. Verotta, S.L. Beal, L.B. Sheiner, Semiparametric approach to pharmacokinetic-pharmacodynamic data, Am. J. Physiol., Regul. Integr. Comp. Physiol. 256 (4) (1989) R1005–R1010.
[44] Victor Virlogeux, Minah Park, Joseph T. Wu, Benjamin J. Cowling, Association between severity of MERS-CoV infection and incubation period, Emerg. Infect. Dis. 22 (3) (2016) 526.
[45] T. Wendling, K. Ogungbenro, E. Pigeolet, S. Dumitras, R. Woessner, L. Aarons, Model-based evaluation of the impact of formulation and food intake on the complex oral absorption of mavoglurant in healthy subjects, Pharm. Res. 32 (5) (2015) 1764–1778.
[46] B. Xiao, G. Wang, W. Li, Radial shifted Legendre moments for image analysis and invariant image recognition, Image Vis. Comput. 32 (12) (2014) 994–1006.